THE JOURNAL OF PHYSICAL CHEMISTRY C

Article

pubs.acs.org/JPCC

Ultrafast Spectroscopy of CdSe Nanocrystals: Morphological and Environmental Effects on Nonradiative and Nonadiabatic Relaxation

Bryan T. Spann and Xianfan Xu*

School of Mechanical Engineering and Birck Nanotechnology Center, Purdue University, West Lafayette, Indiana 47907, United States

ABSTRACT: Ultrafast transient absorption spectroscopy was employed to investigate intraband relaxation and coherent acoustic phonons in quantum dots (QDs) and quantum rods (QRs) of various sizes. We found that the hot electrons and hot holes relaxed through a nonradiative Auger thermalization mechanism that circumvents the phonon bottleneck effect, resulting in sub-2.5 ps intraband relaxation times. The QRs showed an increased intraband relaxation time when compared with QDs as a result of the formation of a 1D exciton along the axial dimension, which partially mitigates the Auger thermalization mechanism. The longer intraband relaxation times for QRs suggest that QRs would act as better sensitizers for hot electron nanocrystal solar cells. The QD samples prepared in thin-film form showed longer intraband relaxation times when compared with their colloidal counterpart; this is a result of the hydrazine treatment used, which mitigates the dominant ligand relaxation pathway for holes. Furthermore, we found that the frequencies of coherent acoustic phonon modes were reduced for both QD and QR thin-film samples as a result of neighboring NC interaction, suggesting that there is a strong dependence on environmental conditions that govern the nonadiabatic relaxation.

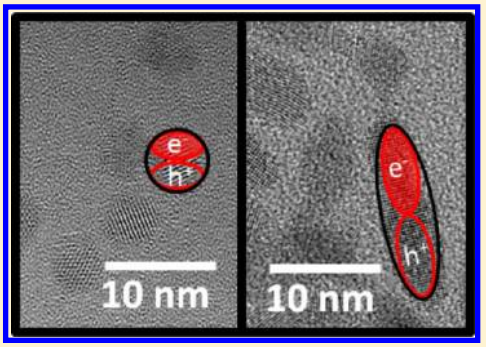

INTRODUCTION

Semiconducting nanocrystals (NCs) exhibit unique electronic structures that have potential to be exploited in various ways. Delicate control of NC size and morphology provides precisely tuned electronic levels between that of molecular and bulk phases.[1] In general, volumetrically smaller NCs facilitate sharper transitions between electronic states, while larger NCs tend toward bulk-like electronic structures, with broadened transitions. NC geometry can also lend itself to electronic transition control.[2] Synthesis of various morphologies has been demonstrated in CdSe, such as quantum dots (QDs),[3] quantum rods (QRs),[4] quantum tetrapods (QTs),[5] and quantum wires (QWs).[6] Through size and morphological control, various novel devices and technologies have come to fruition, for example, nanocrystal solar cells (NCSC),[7] lasers,[8] and LEDs.[9] Here, we focus our study on aspects of NC implementation into solar cells.

Perhaps one of the most intriguing properties of semiconducting NCs is the modification of excited-state electron relaxation. It has been shown in our earlier work as well as by others that the geometrical modifications can directly modify electron relaxation pathways.[6,10−12] For example, by elongating a QD to create a QR, one can maintain quantum confinement in the radial direction, thus controlling the band edge exciton energy, while the axial dimension can be used to control Auger phenomena.[10−12] In particular, we showed previously that QRs show a reduction in the Auger thermalization mechanism, that is, when a high-energy electron scatters its energy with a more massive hole.[12] The Auger thermalization process circumvents the phonon bottleneck effect; therefore, suppressing it is of paramount importance in hot carrier solar cells.

In this work, we build upon our previous efforts[12] to thoroughly investigate the effects of NC confinement, morphology, and environment on excited-state properties using ultrafast transient absorption (TA) spectroscopy. Specifically, we directly compare nonradiative hot exciton relaxation times of three sets of QDs and QRs. The three sets of QDs and QRs are of different sizes; however, each set is controlled such that their band edge energies are similar. By employing this strategy, we can decipher which morphology will have more optimal intraband relaxation times without ambiguity and thus distinguish which morphology will be best suited for NCSC applications. Furthermore, we study both colloidal and thin-film versions of the NCs to establish the differences between NC excited-state properties in suspension and those in an in situ type device environment. By studying the hydrazine-treated thin-film samples, we are able to simultaneously observe the effects of removing the organic ligands from the surface, which have been found to provide a relaxation pathway for the holes in CdSe.[13,14] Finally, we investigate nonadiabatic relaxation by comparing coherent acoustic phonon modes in both the colloidal and thin-film NC environments, which show non-Condon-like behavior in their coherent vibrational modes as a result of neighboring NC interactions.

Received: November 15, 2013
Revised: January 10, 2014
Published: January 12, 2014

dx.doi.org/10.1021/jp4112553 | J. Phys. Chem. C 2014, 118, 2844−2850

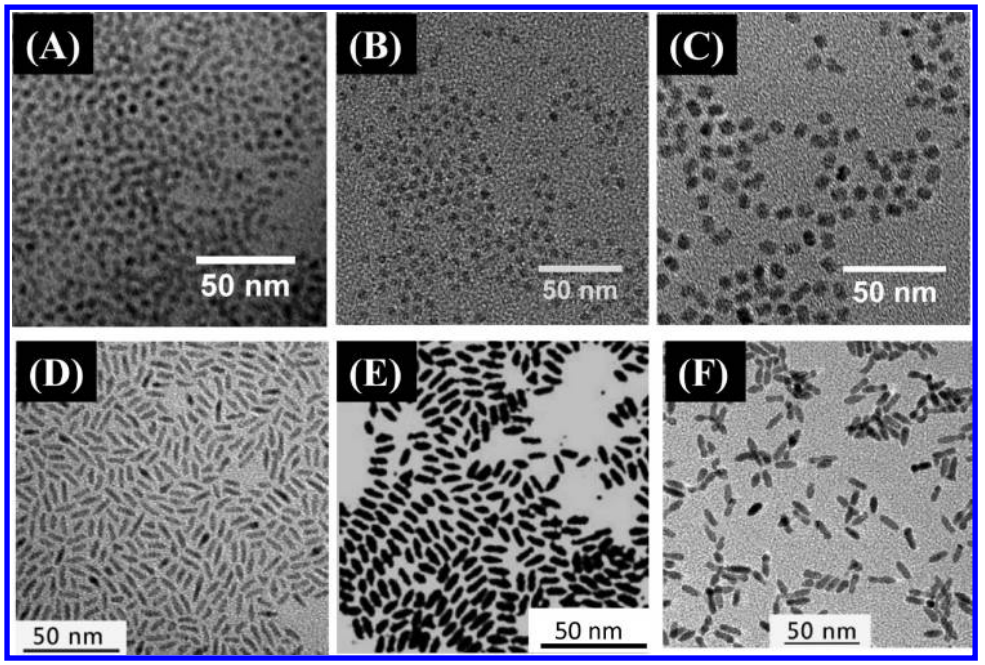

Figure 1. TEM images of QDs (A–C) and QRs (D–F).

EXPERIMENTAL DETAILS

The CdSe NCs were synthesized by NN-Laboratories (Fayetteville, AK, U.S.A.) using wet chemistry techniques such as those described by Murray et al.[3] and Peng et al.[4] QD samples were synthesized with different diameters, each dispersed in toluene solvent and stabilized using surface-attached octadecyl amine (ODA) organic capping ligands. QR samples were synthesized with diameters of approximately 3, 4, and 5 nm and constant lengths of ∼11 nm. The QR samples were stabilized by the following organic capping ligands: octadecanephosphonic acid (ODPA), trioctylphosphine oxide (TOPO), and oleylamine for the 3 nm diameter sample; ODPA and TOPO for the 4 nm diameter sample; and 2-octenoic acid for the 5 nm diameter sample. Sample concentrations were controlled to be 2.5 mg/mL of CdSe to toluene solvent for the colloidal samples.

Details of NC size and morphology were studied by means of high-resolution transmission electron microscopy (HRTEM). Each NC sample was drop-cast from solution onto copper grids for imaging. A Titan 80–300 kV TEM was used for imaging. The crystalline phase was determined by digital image processing from the TEM images (ImageJ software was used).

This work focuses on both colloidal and film forms of sample preparation to test for NC environmental effects on electronic relaxation. Even though many prior studies have focused on colloidal NCs, a vast majority of proposed optoelectronic and solar applications require film-cast NCs rather than colloids.[7−9] To prepare the thin-film samples, the following dip-coating procedure was used: first, a cleaned quartz substrate was dipped into the NC solutions with concentrations of 5.0 mg/mL of CdSe to toluene solvent. Next, it was dipped into a mixture of 30 μL of hydrazine hydrate in 10 mL of deionized water. Finally, it was dipped into 15 mL of acetonitrile for final cleaning. After each dip, a nitrogen gun was used to assist with drying between dipping processes. The aforementioned dip procedure was performed 20 times for each sample.

Linear absorption (LA) and TA spectroscopy was used to investigate ground-state and excited-state electronic properties of the NC samples. A Perkin–Elmer Lambda 950 was used for the LA measurements for both colloidal (2 mm path length cuvette) and thin-film samples. For the TA studies, a two-color pump–probe scheme was employed. The pump and probe beam are derived from a Spectra Physics amplified ultrafast laser system with 70 fs pulses centered at 800 nm with a 5 kHz repetition rate. The probe beam is sent into an optical parametric amplifier (OPA) with a wavelength range from 450 to 2500 nm. The output beam from the OPA is sent to an optical delay stage and is then split into reference and signal beams, with the former going to one side of a balanced photodetector and the latter going through the sample and then into the other side of the balanced photodetector. The pump beam is sent through a barium borate (BBO) crystal to generate frequency-doubled 400 nm light, sent though an optical chopper (500 Hz), and finally focused into the sample. Spot sizes for the pump and probe beams are focused on the samples noncollinearly to $1/e^2$ spot diameters of 320 and 150 μm for the pump and probe, respectively. A low pump fluence of approximately 5 μJ/cm^2 is used to ensure the absence of multiparticle Auger recombination.[7] The balanced photodetector signal is sent to a signal preamplifier and lock-in amplifier for $\sim 10^{-6}$ signal detection ability. Typical scans consist of 20 passes of the optical delay stage while averaging over 1000 pulses per temporal delay step. In addition, colloidal samples are stirred via a magnetic stir bar during each TA experiment to reduce potential photodegradation and charging.[15]

RESULTS AND DISCUSSION

Structural Characterization. The TEM images of QDs and QRs are shown in Figure 1. Upon analyzing the TEM images, the QD samples in Figure 1A–C have diameters of 4.5, 6.0, and 7.4 nm, respectively. The QR samples presented in Figure 1D–F each have lengths of roughly 11 nm and diameters of 3.0, 4.0, and 5.0 nm, respectively. A summary of the synthesized NCs can be found in Table 1, with ±1 standard deviation values based on TEM image analysis.

dx.doi.org/10.1021/jp4112553 | J. Phys. Chem. C 2014, 118, 2844–2850

Table 1. Sample Geometries with ±1 Standard Deviation Values Obtained via TEM Image Analysis

sample	diameter (nm)	length (nm)
QD1	4.5 ± 0.2	na
QD2	6.0 ± 0.4	na
QD3	7.4 ± 0.6	na
QR1	3.0 ± 0.1	11 ± 2
QR2	4.0 ± 0.1	11 ± 2
QR3	5.0 ± 0.2	11 ± 2

HRTEM images were also obtained in order to identify the crystalline phase of the NCs. Representative HRTEM images are presented in Figure 2A and C, with corresponding fast Fourier transform (FFT) data of the QD3 and QR3 samples shown in panels B and D, respectively. All NCs were predominantly in the zinc blende cubic phase. We were able to identify the spacing between adjacent crystal planes as $d \approx 0.35$ nm, which matches well with the standard published data of $d = 0.351$ nm for the (111) planar spacing of zinc blende cubic CdSe.[16]

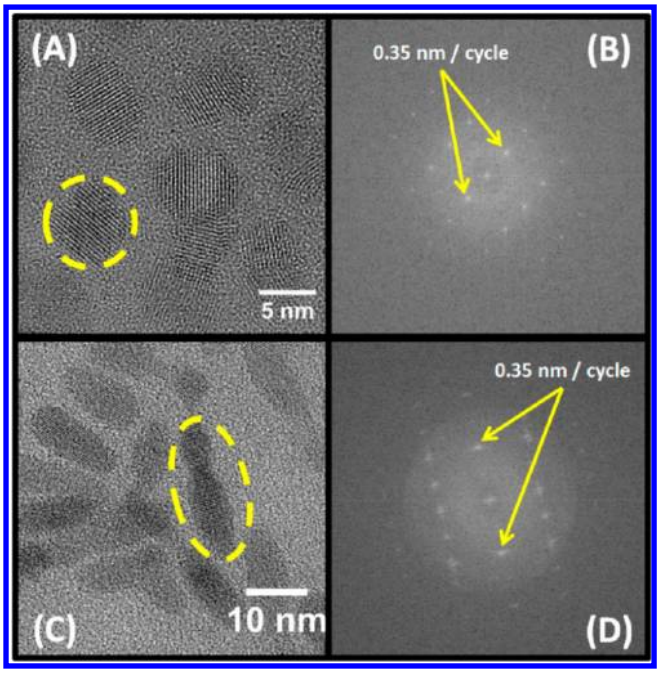

Figure 2. HRTEM images of QD3 (A) with respective FFT data (B) of the selected region shown by the dashed circle. Similarly, (C) shows HRTEM of QR3 with respective FFT data (D) of the selected region shown by the dashed circle.

Optical Characterization. LA data for colloidal and thin-film samples are shown in Figure 3A and B for the QDs and QRs, respectively. In an attempt to directly compare intraband relaxation rates between morphologies, QDs were in fact chosen to match the band edge energies of the QR samples. For example, the peak of the 1S transitions of QD1 is comparable in wavelength to that of QR1, approximately 600 nm, and similarly for QD2−QR2 (~625 nm) and QD3−QR3 (~650 nm). In regard to sample preparation, as illustrated in Figure 3, the film samples show electronic state splitting, as is evident by the broadening near the band edge states; this is likely due to electronic wave function overlap between the closely spaced NCs in the films.[17,18] It should be noted that all spectra in Figure 3 have been normalized to the 1S transition for easy comparison. For reference of scale, each colloidal sample had an absorbance at the 1S transitions of roughly 30 mOD, whereas the thin-film samples had a 10−20 mOD absorbance at the 1S transition.

Intraband Relaxation Studies. We employed TA spectroscopy to understand the ultrafast physical processes in NCs. An important phenomenon during TA spectroscopy measurements is the carrier-induced Stark effect (CISE), which was proposed by Norris et al.[19] and confirmed by others.[12,20] The CISE is the result of spatial confinement of an exciton in NCs, which leads to a DC Stark field in the NC. The DC Stark field causes neighboring electronic transitions to repel one another. It was shown that the CISE can be qualitatively described by the second derivative of the linear absorbance spectra.[20] To illustrate, we calculated the second derivative of the linear absorbance, and an example (QR2 thin-film) is shown in Figure 4A by the dashed line. We then used several probing energies around the 1S transition to query theoretical agreement. Near the band edge energy, the minimum of the second derivative data is marked by B1 for photoinduced bleaching, and the maximum is noted as PA for photoinduced absorption.[20] The results of the TA experiment for the QR2 thin-film sample are shown in Figure 4B and are in agreement with the CISE picture. The blue trend in Figure 3B corresponds to the maximum TA signal. The maximum bleaching signal can be described by the superposition of three indistinguishable photophysical phenomena, stimulated emission, spontaneous

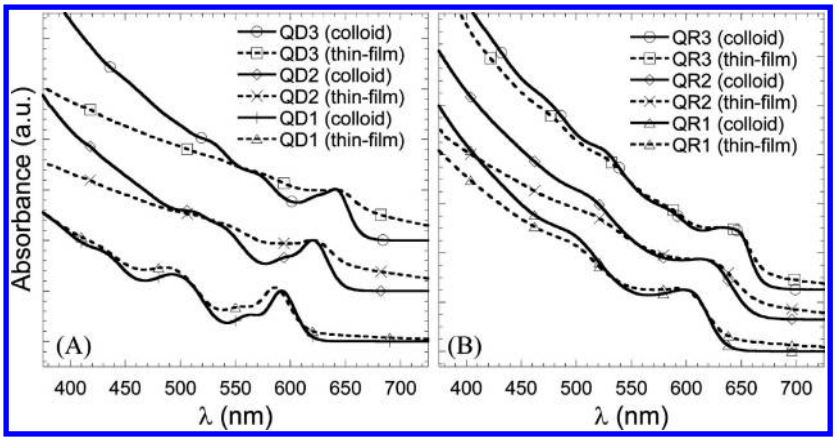

Figure 3. Linear absorbance of colloidal (solid lines) and thin-film (dashed lines) (A) QDs and (B) QRs.

dx.doi.org/10.1021/jp4112553 | J. Phys. Chem. C 2014, 118, 2844−2850

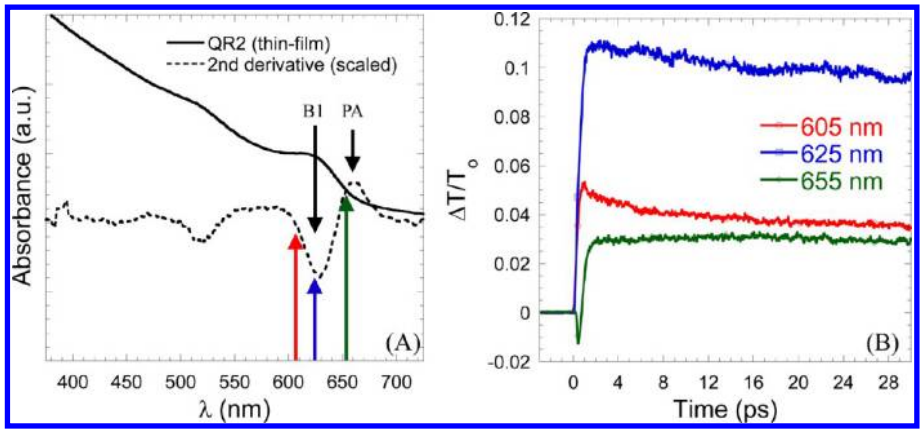

Figure 4. (A) Linear absorbance and second derivative data for the QR2 film with color-coordinated arrows denoting various probing wavelengths used for the TA measurement. (B) The TA experimental results for the probing wavelengths from (A).

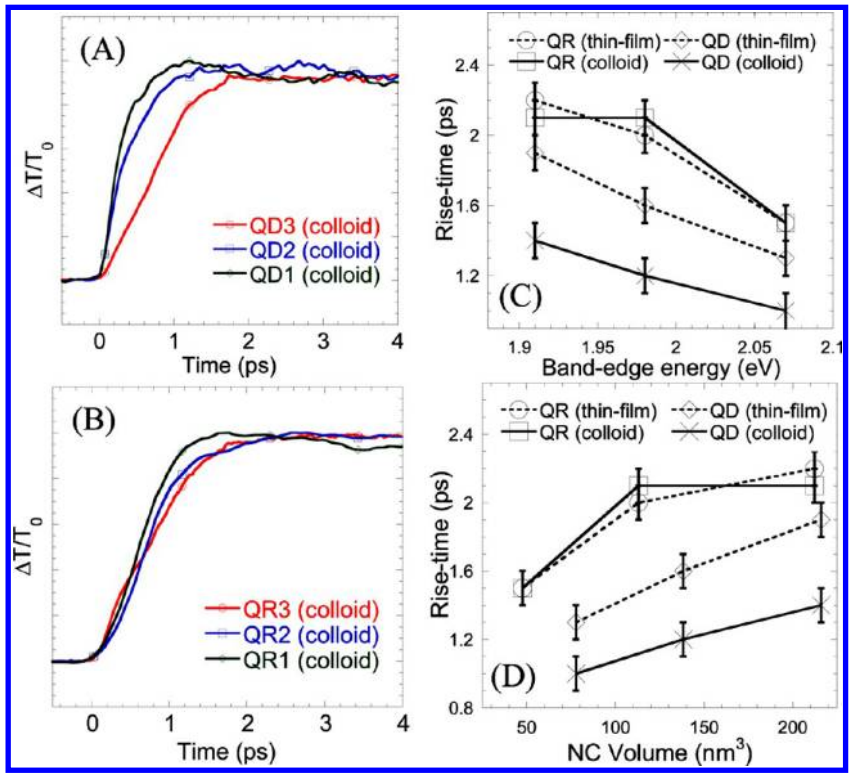

Figure 5. (A,B) TA rise time traces for colloidal QD and QR samples, respectively. (C,D) Rise time data comparison for QD and QR colloidal and thin-film samples with respect to the respective probe energies and NC volume, respectively.

emission, and state-filling induced bleaching (as a result of the Pauli exclusion principle).[13,20] As we probe further to the red to test for PA, we see that there is a negative dip in the TA data, which signifies that once the pump photon has arrived, the CISE causes a red shift in the band edge energy; thus, the lower-energy probe photons can be absorbed. Once this level is saturated, the same three photophysical processes for the B1 probe become possible. All colloid and thin-film samples were tested and were in agreement with the CISE theory and exhibited similar trends to that of the example given in Figure 4.

As mentioned above, an overarching goal of this work is to establish which morphology will work best for NCSCs. This evaluation can be done by comparing intraband relaxation times between the QDs and the QRs. Our experimental design of synthesizing QDs with similar band edge energies as the QRs allows us to compare each set of samples one-by-one, that is, QR1 compared with QD1 and so forth. We can determine the intraband relaxation time by simply considering the rise time of the TA signals for probing energies at the band edge.[20,21] The rise time of the TA data show the time at which the electrons have populated the band edge level and can no longer support additional electrons (as a result of the Pauli exclusion principle). Thus, the TA rise time corresponds to electrons being excited high into the conduction band (CB) followed by intraband relaxation to the band edge. Presented in Figure 5A and B are the results of the TA rise time studies for the colloidal QDs and QRs, respectively. Figure 5C and D provides a more succinct picture of the TA rise time measurements, showing the rise time values for both colloid and thin-film samples with respect to band edge/probing energy and NC volume, respectively.

dx.doi.org/10.1021/jp4112553 | J. Phys. Chem. C 2014, 118, 2844−2850

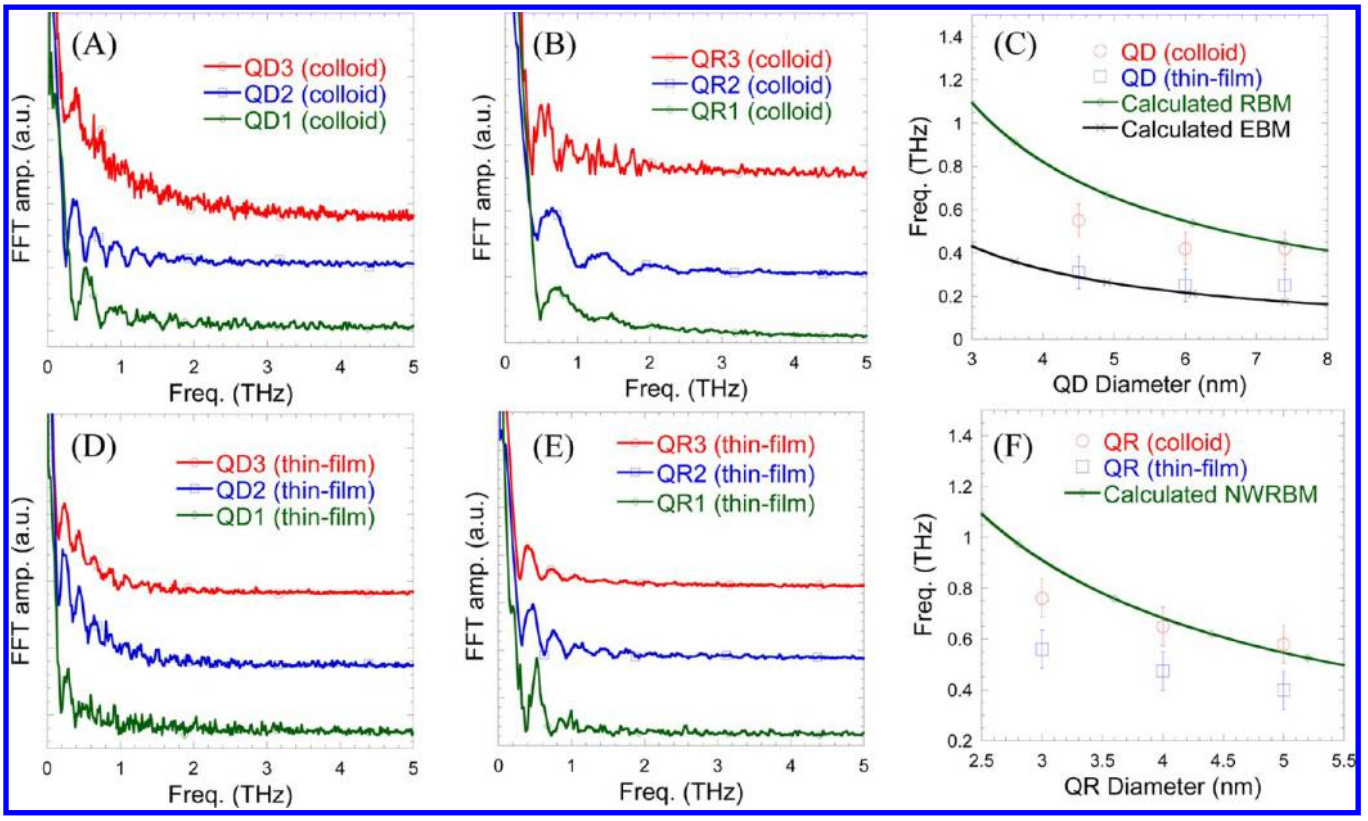

Figure 6. Fourier-transformed TA data probed at the band edge energy for the (A) colloidal QD, (D) thin-film QD, (B) colloidal QR, and (E) thin-film QR. (C,F) Comparisons between the fundamental modes (i.e., the first most intense mode) and calculated modes.

A fundamental reason for considering CdSe NCs as sensitizers in solar cells is because of the predicted phonon bottleneck phenomenon. Theoretically, the phonon bottleneck effect causes hot electrons and hot holes to remain in their excited states for an extended period of time due to the large energy difference between electronic transitions. The large energy spacing requires multiphonon emission for charge carrier relaxation and thus reduces the probability of electronic transition.[1] The phonon bottleneck mediated relaxation time (τ_{PB}) can be approximated by the following expression[1]

$$\tau_{PB} \approx \omega \exp(\Delta E/kT) \quad (1)$$

where ω is the optical phonon frequency (~210 cm^{-1}),[13] ΔE is the energy level spacing between states (~0.1 ev), k is the Boltzmann constant, and T is the temperature. For the NCs studied in this work, eq 1 provides τ_{PB} > 8 ps. As shown in Figure 4C, all samples have relaxation times less than 2.5 ps, signifying that all samples experience exciton relaxation mechanisms that circumvent the phonon bottleneck effect. We believe the mechanism for exciton relaxation to be Auger thermalization for the samples studied here. Auger thermalization occurs when an electron from a high-energy exciton, such as the one generated by the pump photon in the TA experiment, scatters its energy with a hole.[13,22] In CdSe, the valence band (VB) manifold is significantly more dense than that of the CB as a result of the difference in electron and hole effective mass ($m_h \approx 6m_e$). Once the electron inelastically scatters its energy with the hole, it can quickly relax through the dense VB manifold.[23]

As depicted in Figure 5C and D, we find that the QD intraband relaxation times decrease for higher band edge energies and consequently increase with larger NC volumes, consistent with what was found previously.[20] However, by changing the morphology from a spherically symmetric pseudo-zero-dimensional (0D) QD structure to a pseudo-one-dimensional (1D) QR structure, we see an increase in intraband relaxation times for the QR samples, both with respect to band edge energy and NC volume. To explain this increase in intraband relaxation time, we propose similar phenomenological events to those for Auger recombination in NCs. Htoon et al.[10,11] found that the Auger recombination rates were reduced for QRs when compared with similar volume QDs. The Auger recombination decay for QRs was indicative of bimolecular exciton−exciton interactions rather than the three-particle nonradiative relaxation in QDs.[10,11] We propose the same fundamental interaction for Auger thermalization in QRs, that is, the excitons generated become polarized along the length of the QR, which reduces the confinement of the exciton, and thus, the coulomb interaction of the electron and hole for a given bound exciton is reduced and exciton−exciton interactions become more dominant. However, the Auger thermalization mechanism is still evident in the QR samples, as illustrated by QR3 and QR2 having similar intraband relaxation times. This is likely due to the length constraint on the QR samples, which is still in the intermediate confinement regime (CdSe Bohr radius ≈ 5.6 nm).[2] Therefore, extending the length further could potentially increase the intraband relaxation time further for the QR with the same diameter.

The NC environment also appears to have an effect on intraband relaxation, as illustrated by the difference in rise time values for the thin-film and colloidal samples shown in Figure 4C and D. For the QD samples, the thin-film samples show extended relaxation times when compared to their colloidal counterparts. The difference in sample preparation for the QR

dx.doi.org/10.1021/jp4112553 | J. Phys. Chem. C 2014, 118, 2844−2850

samples on intraband relaxation is less significant. For both QDs and QRs, the thin-film samples exhibit intraband relaxation trends qualitatively similar to the colloidal samples with respect to band edge energy and NC volume. The fundamental mechanism behind the increased relaxation time in the QD thin-film samples is likely due to the partial removal of surface ligands. It has been shown by Kambhampati that the organic ligands play an important role in exciton relaxation.[13] Here, we apply a hydrazine treatment to the thin films, which is used to assist with the removal of surface-attached ligands. Furthermore, for QDs, the ligands predominantly affect the hot hole relaxation pathway, while the hot electrons relax predominantly through the Auger thermalization.[13] This further validates our hypothesis of the 1D exciton formation in the QRs, justifying why we see little difference between the colloidal and thin-film samples for the QRs. Due to the 1D exciton formation, the electron and hole will be spatially further from one another, thereby reducing the potential for electron to hole scattering, and because the hole does not receive that energy from the electron, the electron is more likely to relax through the more time-consuming phonon bottleneck pathway. Therefore, the ligands have a relatively smaller contribution to intraband relaxation for the QRs when compared to that for QDs. This also implies that even though different ligands were used to stabilize the QR samples, the intraband relaxations in different samples are not affected.

Aspects of Nonadiabatic Relaxation. In addition to the charge carrier aspects of the TA measurements, we can also extract the superimposed nonadiabatic relaxation, that is, the coherent lattice vibrations. Therefore, we also evaluate the environmental effects on nonadiabatic relaxation, namely, through emission of coherent acoustic phonons. Upon pump photon excitation, a coherent phonon is generated within the NCs. This coherent acoustic phonon is coupled via a piezoelectric and deformation potential; thus, the coherent lattice vibrations deform the lattice, which consequently modulates the band edge energy coherently.[13] For example, small oscillations are visible in the TA signal probed at the band edge of that sample (625 nm), as depicted in Figure 4B.

To analyze the acoustic phonon modes, we computed the FFT of the TA data for each sample (both colloid and thin-film) probed at the band edge energy, and the results are shown in Figure 6. The FFT data show fundamental modes with higher-frequency modes present for each sample. We compare our experimental results with the relevant elastic continuum theory results for vibrating spheres,[24,25] and in doing so, a simple relationship between vibrational frequency (ω_{lm}) and particle size (d) was derived for QDs[25]

$$\omega_{lm} = \frac{S_{lm} v_i}{d} \tag{2}$$

where v_i is either the longitudinal acoustic velocity in CdSe (3570 m/s) or the transverse acoustic velocity in CdSe (1540 m/s). S_{lm} is a constant associated with boundary conditions.[25] For our calculations, we only consider the first two dominant modes; those are the radial breathing mode (RBM, $l = 0$, $m = 1$, 2, 3, ...) and the ellipsoidal breathing mode (EBM, $l = 2$, $m = 1$, 2, 3, ...).[25] For the first-order RBM ($S_{0,1} = 0.92$) and for the first-order EBM ($S_{2,1} = 0.84$), we use the longitudinal acoustic velocity and transverse acoustic velocity in eq 2, respectively.[25] The results of these calculations are shown in Figure 6C. As illustrated in Figure 6C, the colloidal samples match more closely to the RBM, while the thin-film samples match the EBM more closely, suggesting an environmentally dependent nonadiabatic relaxation.

The higher-frequency modes that show up in the FFT spectra in Figure 6A, B, D, and E are not overtones of the first dominant mode, for example, the first-order peak for the colloidal QD2 sample in Figure 6 A is ~0.375 THz; thus, the overtone would be ~0.75 THz. However, the second peak shows a frequency of ~0.625 THz. This suggests that the higher-frequency peaks are physical manifestations. While Saviot et al. observed some evidence of these higher-frequency modes using stimulated Raman spectroscopy,[25] we show a much greater degree of clarity in frequency resolution of higher-frequency modes. However, assigning the higher-order peaks from the FFT to specific physical modes is quite difficult because both the RBM and EBM are possible and higher-order EBM modes can have similar frequencies as lower-order RBM modes;[25] thus, we do not specify each individual higher-order mode resolved by FFT.

For the QR samples, a simple analytic expression is not available; however, an empirical one does exist for nanowires and has been applied successfully to high aspect ratio QRs.[26] The relationship for the nanowire radial breathing mode (NWRBM) for CdSe can be calculated as $\omega_{\mathrm{NWRBM}} = 2.73[\mathrm{THz}\cdot\mathrm{nm}]/d$ and is shown in Figure 6F.[26] Again, for QR samples, the colloids show closer agreement with the NWRBM, while the thin-film samples show a lower-frequency mode. For both the QRs and QDs, the thin-film sample shows a reduction in acoustic phonon frequency, suggesting that there are important environment/non-Condon-like factors modifying the dominant modes. It is difficult to specify the exact physical mechanism modifying the acoustic phonon modes in the films' samples; however, we can gain insight from the work done by Gupalov and Merkulov on NCs in glassy solid matrices.[27] Gupalov and Merkulov showed that when the NCs are prepared in a glassy matrix, the interaction with the neighboring medium will cause reflections of energy carriers from the NC−matrix interface; electronically, this leads to a superposition of the eigenstates of both heavy and light holes, consequently modifying the exciton states. In a similar fashion, this same concept applies to the acoustic eigenmodes of the NC, resulting in a superposition of LA and TA modes.[27] Here, instead of a glassy dielectric matrix that encases individual dots, we have a porous system of NCs that act as the dielectric interfacial medium. The superposition of the LA and TA modes would theoretically red shift the vibrational frequencies, which is precisely what we observe. Another possible mechanism that could be acting simultaneously with the previous explanation is that the NC surface energy changes for the two sample preparation methods. Huxter et al. have shown that the changes in surface energy for NC contribute significantly to modification of elastic properties of the NC.[28] In accordance with this, we expect the thin-film samples to also have altered surface energies when compared to the colloidal samples due to the interaction with other neighboring NCs and the reduction in surface ligands from the hydrazine treatment.

CONCLUSION

Time-resolved ultrafast TA spectroscopy was used to explore the intraband relaxation and coherent acoustic phonons in QDs and QRs of various sizes. We found that intraband relaxation for the NCs was lower than 2.5 ps for all samples, indicating that the NCs experienced Auger thermalization. Furthermore, we showed that QRs had an increased intraband relaxation time

dx.doi.org/10.1021/jp4112553 | J. Phys. Chem. C 2014, 118, 2844−2850

when compared with QDs as a result of the formation of a 1D exciton along the elongated axis of the QR, which reduces the electron to hole scattering potential. Furthermore, the QD samples showed increased intraband relaxation times as a result of the film preparation and hydrazine treatment, which removed (in part) the ligand relaxation pathway for the holes. The longer intraband relaxation times for QRs suggest that they would act as better sensitizers for hot electron NCSCs. In addition, we showed that the thin-film version of the QD samples had longer intraband relaxation times as a result of the hydrazine treatment, which partially removed surface-attached ligands, thus partially eliminating a relaxation pathway for the hot holes. We also found that the coherent acoustic phonons for the colloidal samples of QDs and QRs were in reasonable agreement with the calculated RBM and NWRBM, respectively. However, the coherent acoustic phonon modes become reduced for the thin-film samples for both QDs and QRs. This suggests that there are strong environmental factors that will determine the nonadiabatic relaxation pathway. We believe that the frequency reduction is a result of the superposition of LA and TA acoustic eigenmodes as a result of neighboring NC interaction. Furthermore, frequency modification could also be due in part to changes in surface energy for the NCs when prepared in the thin-film form without surface-attached ligands.

AUTHOR INFORMATION

Corresponding Author

*E-mail: xxu@purdue.edu.

Notes

The authors declare no competing financial interest.

ACKNOWLEDGMENTS

Support for this work was provided by the National Science Foundation and is gratefully acknowledged. We also thank NN-Laboratories, Dr. A. Garrelts, and Dr. S. Suslov for assistance with TEM images. Finally, we thank K. Rickey for helpful discussions regarding thin-film sample preparation.

REFERENCES

(1) Nozik, A. Spectroscopy and Hot Electron Relaxation Dynamics in Semiconductor Quantum Wells and Quantum Dots. *Annu. Rev. Phys. Chem.* **2001**, *52*, 193−231.

(2) Katz, D.; Wizansky, T.; Millo, O.; Rothenberg, E.; Mokari, T.; Banin, U. Size-Dependent Tunneling and Optical Spectroscopy of CdSe Quantum Rods. *Phys. Rev. Lett.* **2002**, *89*, 086801/1−086801/4.

(3) Murray, C.; Norris, D.; Bawendi, M. Synthesis and Characterization of Nearly Monodisperse CdE (E = Sulfur, Selenium, Tellurium) Semiconductor Nanocrystallites. *J. Am. Chem. Soc.* **1993**, *115*, 8706−8715.

(4) Peng, X.; Manna, L.; Yang, W.; Wickham, J.; Scher, E.; Kadavanich, A.; Alivisatos, A. Shape Control of CdSe Nanocrystals. *Nature* **2000**, *404*, 59−61.

(5) Shieh, F.; Saunders, A. E.; Korgel, B. A. General Shape Control of Colloidal CdS, CdSe, CdTe Quantum Rods and Quantum Rod Heterostructures. *J. Phys. Chem. B* **2005**, *109*, 8538−8542.

(6) Robel, I.; Bunker, B. A.; Kamat, P. V.; Kuno, M. Exciton Recombination Dynamics in CdSe Nanowires: Bimolecular to Three-Carrier Auger Kinetics. *Nano Lett.* **2006**, *6*, 1344−1349.

(7) Robel, I.; Subramanian, V.; Kuno, M.; Kamat, P. V. Quantum Dot Solar Cells. Harvesting Light Energy with CdSe Nanocrystals Molecularly Linked to Mesoscopic TiO_2 Films. *J. Am. Chem. Soc.* **2006**, *128*, 2385−2393.

(8) Klimov, V. I. Optical Gain and Stimulated Emission in Nanocrystal Quantum Dots. *Science* **2000**, *290*, 314−317.

(9) Kim, T.; Cho, K.; Lee, E.; Lee, S.; Chae, J. Full-Colour Quantum Dot Displays Fabricated by Transfer Printing. *Nat. Photonics* **2011**, *5*, 176−182.

(10) Htoon, H.; Hollingsworth, J. A.; Dickerson, R.; Klimov, V. I. Effect of Zero- to One-Dimensional Transformation on Multiparticle Auger Recombination in Semiconductor Quantum Rods. *Phys. Rev. Lett.* **2003**, *91*, 227401/1−227401/4.

(11) Htoon, H.; Hollingworth, J. A.; Malko, A. V.; Dickerson, R.; Klimov, V. I. Light Amplification in Semiconductor Nanocrystals: Quantum Rods versus Quantum Dots. *Appl. Phys. Lett.* **2003**, *82*, 4776−4778.

(12) Spann, B. T.; Chen, L.; Ruan, X.; Xu, X. Energy Relaxation in CdSe Nanocrystals: The Effects of Morphology and Film Preparation. *Opt. Express* **2013**, *21*, 1018−1024.

(13) Kambhampati, P. Hot Exciton Relaxation Dynamics in Semiconductor Quantum Dots: Radiationless Transitions on the Nanoscale. *J. Phys. Chem. C* **2011**, *115*, 22089−22109.

(14) Kambhampati, P. Unraveling the Structure and Dynamics of Excitons in Semiconductor Quantum Dots. *Acc. Chem. Res.* **2011**, *44*, 1−13.

(15) Taguchi, S.; Saruyama, M.; Teranishi, T.; Kanemitsu, Y. Quantized Auger Recombination of Biexcitons in CdSe Nanorods Studied by Time-Resolved Photoluminescence and Transient-Absorption Spectroscopy. *Phys. Rev. B* **2011**, *83*, 155324/1−155324/7.

(16) JCPDS Data File No. 19-191.

(17) Schedelbeck, G.; Wegscheider, W.; Bichler, M.; Abstreiter, G. Coupled Quantum Dots Fabricated by Cleaved Edge Overgrowth: From Artificial Atoms to Molecules. *Science* **1997**, *278*, 1792−1795.

(18) Luther, J. M.; Beard, M. C.; Song, Q.; Law, M.; Ellingson, R. J.; Nozik, A. J. Multiple Exciton Generation in Films of Electronically Coupled PbSe Quantum Dots. *Nano Lett.* **2007**, *7*, 1779−1784.

(19) Norris, D.; Sacra, A.; Murray, C.; Bawendi, M. Measurement of the Size Dependent Hole Spectrum in CdSe Quantum Dots. *Phys. Rev. Lett.* **1994**, *72*, 2612−2615.

(20) Klimov, V. I. Optical Nonlinearities and Ultrafast Carrier Dynamics in Semiconductor Nanocrystals. *J. Phys. Chem. B* **2000**, *104*, 6112−6123.

(21) Mohamed, M. B.; Burda, C.; El-Sayed, M. A. Shape Dependent Ultrafast Relaxation Dynamics of CdSe Nanocrystals: Nanorods vs Nanodots. *Nano Lett.* **2001**, *1*, 589−593.

(22) Wang, L.-W.; Califano, M.; Zunger, A.; Franceschetti, A. Pseudopotential Theory of Auger Processes in CdSe Quantum Dots. *Phys. Rev. Lett.* **2003**, *91*, 056404/1−056404/4.

(23) Efros, A.; Kharchenko, V.; Rosen, M. Breaking the Phonon Bottleneck in Nanometer Quantum Dots: Role of Auger-Like Processes. *Solid State Commun.* **1995**, *93*, 281−284.

(24) Saviot, L.; Murray, D. Long Lived Acoustic Vibrational Modes of an Embedded Nanoparticle. *Phys. Rev. Lett.* **2004**, *93*, 055506/1−055506/4.

(25) Saviot, L.; Champagnon, B.; Duval, E.; Kudriavtsev, I. A.; Ekimov, A. I. Size Dependence of Acoustic and Optical Vibrational Modes of CdSe Nanocrystals in Glasses. *J. Non. Cryst. Solids* **1996**, *197*, 238−246.

(26) Lange, H.; Mohr, M.; Artemyev, M.; Woggon, U.; Thomsen, C. Direct Observation of the Radial Breathing Mode in CdSe Nanorods. *Nano Lett.* **2008**, *8*, 4614−4617.

(27) Gupalov, S.; Merkulov, I. Theory of Raman Light Scattering by Nanocrystal Acoustic Vibrations. *Phys. Solid State* **1999**, *41*, 1349−1358.

(28) Huxter, V. M.; Lee, A.; Lo, S. S.; Scholes, G. D. CdSe Nanoparticle Elasticity and Surface Energy. *Nano Lett.* **2009**, *9*, 405−409.

NOTE ADDED AFTER ASAP PUBLICATION

This article was published ASAP on January 22, 2014. Figure 6 has been revised. The correct version was published on January 28, 2014.